Axial compression behavior and stress–strain modeling of CFRP-confined square RC columns with varying anchor configurations

Zhang, Zhengxie; Zheng, Yonglai; Pan, Tanbo; Hou, Chenyu; Lan, Xin; Xu, Xubing; Wu, Liangqin; Yang, Chao; Zhou, Yubao

DOI
10.1016/j.engstruct.2025.121456

Publication date
2025

Document Version
Final published version

Published in
Engineering Structures

Citation (APA)
Zhang, Z., Zheng, Y., Pan, T., Hou, C., Lan, X., Xu, X., Wu, L., Yang, C., & Zhou, Y. (2025). Axial compression behavior and stress–strain modeling of CFRP-confined square RC columns with varying anchor configurations. *Engineering Structures*, *345*, Article 121456. https://doi.org/10.1016/j.engstruct.2025.121456

Engineering Structures 345 (2025) 121456

Contents lists available at ScienceDirect

Engineering Structures

journal homepage: www.elsevier.com/locate/engstruct

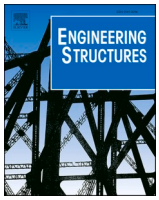

Axial compression behavior and stress–strain modeling of CFRP-confined square RC columns with varying anchor configurations

Zhengxie Zhang [a], Yonglai Zheng [a], Tanbo Pan [b,*], Chenyu Hou [a], Xin Lan [a], Xubing Xu [a], Liangqin Wu [b], Chao Yang [b], Yubao Zhou [c]

[a] Department of Hydraulic Engineering, College of Civil Engineering, Tongji University, China
[b] Department of Bridge Engineering, College of Civil Engineering and Architecture, East China Jiaotong University, China
[c] Faculty of Civil Engineering and Geosciences, Delft University of Technology, the Netherlands

ARTICLE INFO

Keywords:
CFRP anchorage system
Confined
RC square columns
Stress-strain model

ABSTRACT

Carbon fiber reinforced polymer (CFRP) has emerged as an effective material for strengthening reinforced concrete (RC) structures due to its high tensile strength, corrosion resistance, and ease of installation. However, in square or rectangular RC columns, stress concentrations at corners hinder the development of uniform confinement, thereby reducing strengthening efficiency. This study presents a comprehensive experimental and theoretical investigation into the performance of CFRP-confined RC square columns with varying anchor configurations. Six full-scale column specimens were tested under monotonic axial compression, each externally wrapped with one layer of CFRP sheet and installed with zero to four CFRP anchors. All columns were chamfered with a 30 mm radius to mitigate corner stress concentrations. The experimental results demonstrated that CFRP anchors significantly enhanced load-bearing capacity and ductility, improved lateral confinement, and modified the failure mechanisms. The specimen with three anchors exhibited optimal performance, with a 51.5 % increase in peak load (from 879.9 kN to 1333.2 kN) and a 29.9 % improvement in ductility index compared to the unconfined control. The failure mode transitioned from brittle global instability to ductile localized damage, accompanied by more uniform hoop strain distribution. However, excessive anchoring introduced stress interference and local cracking, leading to performance degradation. To characterize the mechanical response, a modified stress–strain model was developed, incorporating a reduction factor to account for confinement weakening caused by anchor installation. The model exhibited strong agreement with experimental data ($R^2 >$ 87 %) in predicting both peak and ultimate stresses. This study provides valuable insights into the mechanical enhancement mechanisms of CFRP anchoring systems and offers a rational design basis for strengthening non-circular RC columns in structural rehabilitation.

1. Introduction

With the rapid advancement of urban development, many existing concrete structures have significantly exceeded their original design service life, leading to increasing concerns regarding their load-bearing capacity and durability. Consequently, the demand for structural strengthening and rehabilitation has grown substantially. Traditional strengthening techniques—such as steel plate bonding and section enlargement—often suffer from several limitations, including complex construction procedures, increased self-weight, and poor corrosion resistance, making them less suitable for modern structures that require high performance, lightweight properties, and long-term durability. In this context, fiber-reinforced polymer (FRP) has emerged as a key material for concrete strengthening due to its high specific strength, excellent corrosion resistance, and ease of application [1–3]. The widespread adoption of FRP composites has not only improved the load-bearing and ductility performance of structures but also accelerated the development of composite materials in the field of civil engineering [4–6]. As a result, investigating the strengthening mechanisms and performance enhancement strategies for concrete structures has become a critical research focus at the intersection of structural engineering and materials science.

The external wrapping technique using CFRPs has been widely applied to strengthen various concrete structural elements, including

* Corresponding author.
E-mail address: 1830149@tongji.edu.cn (T. Pan).

https://doi.org/10.1016/j.engstruct.2025.121456
Received 11 May 2025; Received in revised form 23 September 2025; Accepted 24 September 2025
Available online 29 September 2025

beams, columns, and walls. In particular, it has demonstrated excellent effectiveness in enhancing the compressive performance of column members. Extensive research has shown that FRP sheets can provide lateral confinement to the concrete core, thereby generating a triaxial compressive stress state that significantly improves both the ultimate load capacity and plastic deformation ability of the confined members [7,8]. Bai et al. [9] investigated the interaction between longitudinal reinforcement buckling and FRP wrapping in RC columns, highlighting the significant influence of corner radius and number of FRP layers on compressive performance. Increasing the corner radius and the number of wrapping layers improved the confinement efficiency. Al-Nimry and Neqresh [10] examined the effect of CFRP sheets on square RC columns under eccentric loading and found that CFRP wrapping significantly enhanced both axial and flexural capacities, particularly improving ductility and toughness under large eccentricities. Fan et al. [11,12] developed a meso-scale finite element model for CFRP-confined rectangular RC columns, revealing that the plastic hinge length is highly sensitive to corner radius and confinement ratio. Larger sizes resulted in increased prediction error, although greater corner radii effectively mitigated this issue. Rehman et al. [13] reported that while CFRP wrapping improved the load-bearing capacity and ductility of pre-damaged RC columns, its stiffness recovery was limited, indicating a need for enhanced strengthening techniques under specific service conditions. Compared to circular columns, rectangular or square sections are more prone to stress concentration at the corners, where FRP sheets often exhibit premature debonding or rupture. This limits the full development of confinement [14–16]. Therefore, improving the efficiency of FRP confinement in non-circular cross-sections remains a key challenge in current research.

To enhance the interfacial bonding performance and confinement stability of FRP in the strengthening of rectangular concrete members, various composite reinforcement strategies have been proposed by researchers [17–19]. Saleem et al. [20] conducted systematic experiments on concrete columns confined with cotton fiber rope (CFRRP) and nylon fiber rope (NFRRP), evaluating their compressive behavior and stress–strain responses under different aspect ratios and corner radii. Kunawisarut et al. [21] showed that unidirectional jute FRP (UJFRP) markedly improves concrete strength and ductility over woven jute FRP (WJFRP) and proposed a simplified model for accurate prediction of ultimate stress and strain. Zhong et al. [22] investigated the axial compressive performance of rectangular FRP–concrete–high-strength steel multi-tube composite columns (RMTCCs), revealing that compared with conventional RCFFT columns, RMTCCs exhibit significantly improved load capacity and ductility, while mitigating post-peak softening caused by insufficient FRP confinement. Among various techniques, anchorage systems composed of FRP anchors or dowels have proven particularly effective in preventing FRP sheet debonding and enhancing interfacial shear transfer, making them a promising solution for improving overall strengthening efficiency [23,24]. Existing studies indicate that FRP anchoring systems offer clear advantages in improving force transfer between the FRP and concrete, delaying interfacial failure, and enhancing structural ductility [25–27]. Triantafillou et al. [28] systematically examined the influence of section aspect ratio, anchorage type and quantity, local reinforcement, and section enlargement on the axial compressive behavior of FRP-confined RC columns, highlighting that properly embedded anchors can nearly double the confinement effect, and local edge reinforcement can further increase confinement efficiency by approximately 50 %. Gao et al. [29] studied the seismic performance of RC square columns strengthened with fan-shaped anchors and bidirectional BFRP composite laminates under low-cycle reversed loading. The results showed that anchorage significantly improved the working strain in longitudinal fibers and enhanced bending performance. Tasdemir et al. [30] conducted field tests to investigate the effects of anchor diameter, hole depth, fan angle, and fan-shaped confinement on anchorage capacity and failure modes, emphasizing that fiber alignment and anti-peeling measures significantly enhance anchorage performance. However, since CFRP anchors are embedded into the concrete through drilled holes, the installation process may introduce local stress concentrations and compromise the structural integrity. Therefore, the rational configuration of anchorage parameters—such as anchor quantity, layout, and dimensions—remains unclear. A deeper understanding of their influence on structural behavior still requires systematic experimental investigation and theoretical analysis.

Regarding the mechanical behavior of concrete columns strengthened with FRP anchoring systems, several theoretical models have been developed based on the principle of confinement stress superposition. These models typically treat the confining effects of FRP sheets, anchors, and transverse reinforcement in an equivalent manner to establish a unified expression for lateral confinement pressure, which is then used to predict the stress–strain behavior of the strengthened concrete. Saeed et al. [19] conducted systematic pull-out tests on FRP anchors fabricated from CFRP ropes, thoroughly analyzing the effects of embedment depth, hole diameter, and epoxy type on anchorage capacity and failure modes. They introduced a modified pull-out performance model specifically applicable to column strengthening scenarios. Zhou and Wu [31] proposed a unified constitutive model with high generality and clear physical interpretation, capable of accurately describing the stress–-strain and bond–slip relationships in concrete–FRP composite systems, effectively replacing multiple existing empirical models. Del Rey Castillo et al. [32] performed seismic performance tests on RC columns flexibly strengthened with FRP, validating the accuracy of combined FRP anchorage and wrapping in predicting moment capacity. They further identified a three-stage nonlinear response and proposed a trilinear model based on distinct failure modes of anchors and FRP sheets. Bournas et al. [33], through comparative tests involving various anchorage parameters (e.g., number, diameter, sheet type, and adhesive), identified fiber rupture as the most desirable failure mode and quantitatively correlated effective strain with confinement stress. Hany et al. [34] conducted cyclic axial loading tests on rectangular columns strengthened with externally bonded CFRP sheets and anchors, developing an envelope model comprising a pre-peak parabolic and post-peak linear segment. A full cyclic response model incorporating unloading–reloading paths was also established. Lin, Teng, and colleagues [35] proposed a novel stress–strain model for FRP-confined concrete based on finite element analysis and equivalent circular section mapping. By introducing a stress ratio parameter and a corner strain-driven mechanism, the model significantly improved post-peak prediction accuracy. Isleem et al. [36,37] developed a unified axial stress–strain model for rectangular RC columns simultaneously confined by FRP wrapping and anchorage, based on axial compression test data. The model features a three-segment structure and a composite confinement stress formulation, effectively capturing bilinear and post-peak softening responses under varying confinement conditions. However, most existing theoretical models do not adequately account for the local weakening of concrete strength caused by an increasing number of anchors, nor do they provide detailed simulations of interfacial slip, bond failure, or localized stress concentration. Under high-density anchor cluster configurations, existing models struggle to capture the nonlinear variation in peak strength, limiting their applicability in optimal strengthening design and practical engineering applications.

In summary, although CFRP anchoring systems have demonstrated clear advantages in enhancing structural strengthening efficiency, key gaps remain regarding the optimal anchor configuration and theoretical modeling, particularly for rectangular RC columns. To address these challenges, this study conducted monotonic axial compression tests on six full-scale RC square column specimens. The specimens were strengthened by external CFRP wrapping with varying numbers of CFRP anchors (ranging from zero to four). Through detailed measurements of load–displacement behavior, hoop strain distribution, and stress–strain responses, the effects of anchor quantity on structural performance were systematically evaluated. Furthermore, a modified stress–strain model

incorporating the weakening effect caused by anchor installation was proposed to improve predictive accuracy. The findings aim to guide the optimization and engineering application of CFRP anchoring systems in strengthening non-circular RC columns.

2. Experimental program

2.1. Specimen design

The experimental program comprised monotonic uniaxial compression tests on six RC short columns. Each specimen had a height of 400 mm and a rectangular cross-section measuring 150 mm × 150 mm. All specimens were cast using C30 concrete. Longitudinal reinforcement consisted of four 12 mm diameter HPB300-grade steel bars, while transverse reinforcement was provided by 8 mm HPB300-grade stirrups spaced at 120 mm intervals. The clear concrete cover was 20 mm. The detailed dimensions and reinforcement layout of the specimens are illustrated in Fig. 1.

This experimental program aims to investigate the effects of different CFRP anchor configurations on the confinement performance of RC columns. Specifically, the study examines how varying the number of CFRP anchors influences the strengthening effectiveness of RC short columns. Previous studies have shown that chamfering the corners of non-circular columns prior to CFRP application can effectively reduce stress concentrations. Moreover, the confinement efficiency generally improves with increasing chamfer radius. According to the literature, typical chamfer radii range from 20 mm to 30 mm, with enhanced performance sometimes observed when the radius is increased to 35 mm–45 mm. In the present study, a chamfer radius of 30 mm—commonly considered optimal under standard conditions—was applied to all specimens. Additionally, each strengthened RC column was fully wrapped with a single layer of CFRP. The anchor bolts were positioned at the midpoints of each side of the column specimens and evenly spaced along the longitudinal axis according to their quantity. UU denotes the unreinforced control; S0, CFRP wrap without bolts; and S1–S4, one to four bolts per side. Detailed configurations of all specimens are provided in Table 1.

2.2. Material properties

The concrete employed for the RC square columns was designed to achieve a target unconfined compressive strength of 30 MPa, with a specified water–cement ratio of 0.52. The proportion of concrete is cement, sand, stone and water. During the casting process, three sets of concrete cubes with different strength grades, each measuring 150 mm × 150 mm × 150 mm, were prepared. These cubes were cured under the same conditions as the main specimens and were tested for compressive strength at the time of specimen testing. The reinforcement consisted of hot-rolled ribbed steel bars with a diameter of 12 mm (HPB300) and a nominal yield strength of 300 MPa. Longitudinal reinforcement was fixed in place using stirrups prior to concrete casting. The CFRP utilized in this study was a unidirectional carbon fiber fabric supplied by a manufacturer based in Shanghai. For fiber impregnation, a two-component modified epoxy resin, also produced by a Shanghai-based company, was applied. The detailed material properties of the concrete, steel reinforcement, CFRP, and epoxy resin used in this experiment are summarized in Table 2.

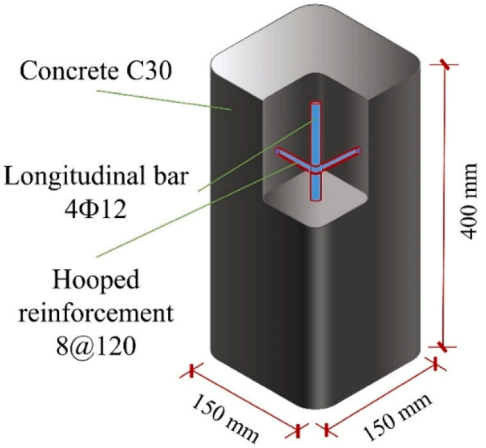

Fig. 1. Dimensions and reinforcement details of the test specimens.

Table 1
Detailed configuration of the test specimens.

Specimen number	CFRP sheet	Anchor number	Anchor depth /mm	Fan length[a] /mm
UU	0	0	0	—
S0	1	0	0	—
S1	1	1	35	60
S2	1	2	35	60
S3	1	3	35	60
S4	1	4	35	60

[a] The radius length of the anchor fan.

2.3. Installation of the CFRP anchorage system

(1) Fabrication Procedure of CFRP Anchors

The fabrication of CFRP anchors in this study followed the procedure proposed by Kim & Smith [38], and the test results indicated a tensile strength of 3800 MPa with a maximum tensile capacity of 26.68 kN. The CFRP anchors were fabricated using unidirectional CFRP sheets, each anchor was prepared by cutting a strip measuring 150 mm in width and 95 mm in length. The length consisted of a 60 mm fan-shaped portion and a 35 mm embedded segment, which included a small edge folded to form a 90° bend. The cut CFRP sheet was then rolled into a tubular shape. To prevent damage at the bent segment, the hardened portion was limited to no more than two-thirds of the embedded length. Epoxy resin was applied at the end of the anchor to form a hardened axial section, ensuring adequate strength and durability. The resulting anchor had a butterfly-shaped configuration with a nominal diameter of 10 mm. The detailed fabrication process of the CFRP anchors is illustrated in Fig. 2.

(2) Installation of the CFRP Anchoring System

Anchor holes were drilled along the midlines of all four faces of the specimen, with a diameter of 10 mm and a depth matching the embedded length of the CFRP anchor (35 mm). To ensure that the CFRP anchoring system effectively restrained deformations and cracking induced by loading, the holes were thoroughly cleaned to remove dust and debris. The specimen surfaces were then ground using an angle grinder and wiped multiple times with acetone to eliminate surface contaminants. Prior to application, components A and B of the two-part epoxy resin were thoroughly mixed. The mixed resin was uniformly applied to both the specimen surface and the interior of the drilled holes. A layer of CFRP fabric was then bonded onto the concrete surface, covering the anchor holes. Each CFRP anchor was inserted through the fabric and embedded into the holes. The exposed end of the anchor was unfolded into a fan shape and pressed tightly against the CFRP sheet to ensure full contact and bonding. After installation, the surface of the specimen was smoothed to remove air bubbles introduced during the bonding process, thereby preventing the formation of any defective interfacial zones within the CFRP anchoring system. The detailed installation procedure is illustrated in Fig. 3.

After installation, the strengthened specimens were placed in a temperature-controlled indoor environment to allow the initial setting

Table 2
Material properties of concrete, steel reinforcement, CFRP, and epoxy resin used in the experiment.

Material	Material parameter					
Concrete	$f_{cu,k}$ (MPa)				f_c' (MPa)	
	34.8				39.4 ± 1.9	
Steel bar	Rebar Grade	Diameter (mm)	Yield strength f_y (N/mm^2)	Ultimate tensile strength f_u (N/mm^2)	Modulus of elasticity E_s (10^5N/mm^2)	
	HPB300	12	452.15	615.72	2.01	
CFRP	Areal Density (g/m^2)	Tensile Strength (Mpa)	Elastic Modulus (Gpa)	Elongation at Break (%)	Interlaminar Shear Strength (Mpa)	
	200	3325	2.40×10^5	1.74	45.1	
Epoxy resin	Tensile Strength (Mpa)	Compressive Strength (Mpa)	Tensile Modulus of Elasticity (Mpa)	Flexural Strength(Mpa)	Elongation (%)	Tensile Shear Strength (Mpa)
	50.9	82.3	3300	75.3	1.94	18.8

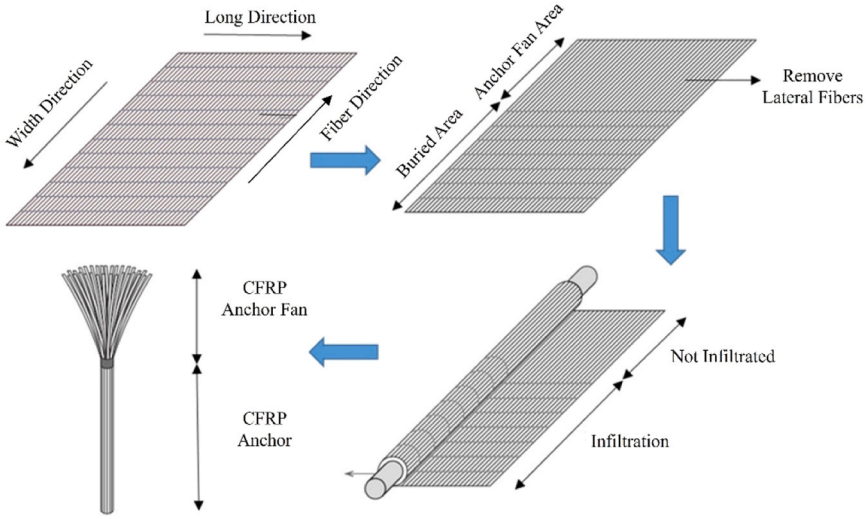

Fig. 2. Fabrication process of the CFRP anchors.

of the CFRP anchoring system. After 24 h, the protruding discrete fibers at the ends of the CFRP sheets were trimmed, and the specimen surfaces were cleaned using non-woven fabric. Subsequently, the specimens were cured under stable ambient conditions for an additional 7 days to ensure full hardening of the CFRP anchoring system. Fig. 4 illustrates the layout of the CFRP anchoring system.

2.4. Instrumentation set up

The experimental tests were conducted using a high-stiffness full-range compression testing machine at Tongji University. The testing setup is illustrated in Fig. 5. The main technical specifications of the machine are as follows: maximum load capacity of 3000 kN; maximum vertical clearance of 850 mm; load measurement accuracy within ±1 % of the indicated value; displacement measurement accuracy within ±0.1 % F.S.; loading rate adjustable from 0 % to 100 % F.S./min; and displacement rate ranging from 0.001 to 50 mm/min. This testing system enables real-time acquisition of fundamental mechanical parameters such as compressive strength, full stress–strain curves, and elastic modulus.

All specimens were tested under uniaxial compression until failure, using load control with a constant loading rate of 150 kN/min. To monitor the axial strain during loading, four displacement transducers (with a measurement range of 250 mm) were installed on each specimen—two positioned on the upper platen and two on the lower platen of the testing machine. The average of the readings from the two pairs of transducers was used to calculate the axial strain during compression. In addition, eight circumferential electrical strain gauges and two axial strain gauges were affixed around the mid-height of each specimen to monitor hoop and axial strains during the compression process. For rectangular specimens, where CFRP sheets are prone to tensile rupture at corner regions due to stress concentration caused by curvature changes, four additional strain gauges were installed at the corners at mid-height. The circumferential strain gauges had a gauge length of

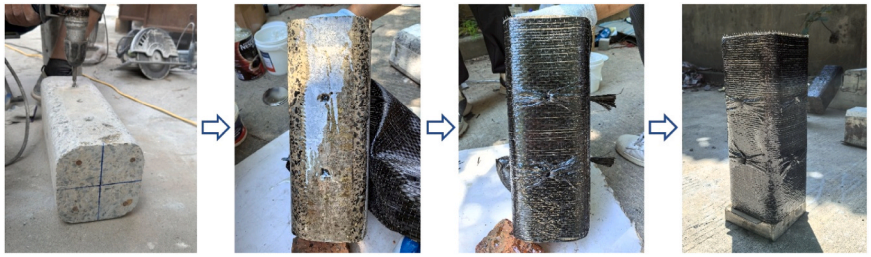

Fig. 3. Installation process of the CFRP anchoring system.

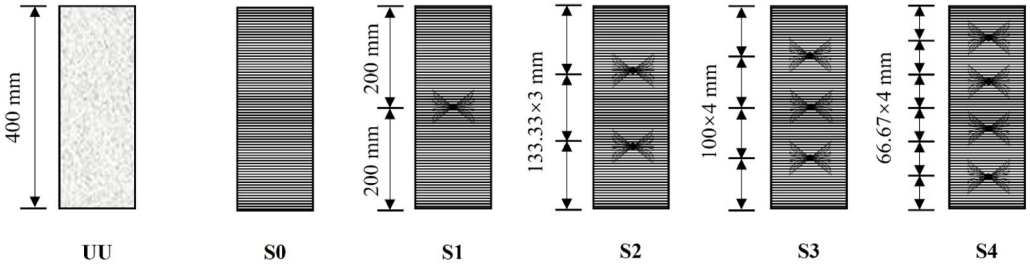

Fig. 4. Layout form of CFRP anchoring system.

50 mm, while the corner and axial strain gauges were 20 mm in length to minimize measurement errors. Axial strain for stress–strain curves was obtained from the strain gauge on the failure side, while gauges on both sides were installed to prevent data loss or invalid readings. The detailed layout of the displacement transducers and strain gauges is illustrated in Fig. 6.

3. Experimental results

3.1. Failure modes

Fig. 7 illustrates the failure patterns of RC columns strengthened with different numbers of CFRP anchors under uniaxial compression. The control specimen (UU) exhibited a typical brittle failure mode, characterized by spalling of the concrete cover, corner cracking, buckling of longitudinal reinforcement, and severe crushing of the concrete core. At the initial stage of loading, due to the absence of effective confinement, the tensile strength of concrete was insufficient to resist cracking at the corners, which initiated early failure. As the cracks propagated, the concrete cover delaminated, indicating that the integrity of the protective layer could not be maintained under the ultimate load. The emergence of localized damage further accelerated the deterioration process. With the development of cracking, the embedded steel bars gradually became exposed and entered a plastic deformation phase. Owing to the limited lateral confinement provided by the concrete, corner cracking intensified, and the axial load carried by the longitudinal reinforcement at the top of the specimen increased, leading to local buckling of the steel bars. This significantly hastened the final failure of the specimen.

In contrast, the specimens strengthened with CFRP exhibited improved confinement due to the restraining effect of the CFRP sheets, which effectively suppressed lateral expansion of the concrete, delayed crack propagation, and enhanced the overall ductility of the structure. For specimen S0, the failure mode was characterized by longitudinal cracking, slight buckling of the steel bars, and localized rupture of the CFRP confinement layer. Although the CFRP wrapping enhanced both the ultimate load-carrying capacity and deformation capacity of the specimen, the confinement was not uniformly distributed. In corner regions and areas with suboptimal bonding quality, the CFRP failed due to tensile stress exceeding its ultimate strength, resulting in a loss of confinement. Consequently, the concrete cover spalled off, and mild buckling of the longitudinal reinforcement occurred, leading to localized structural instability under high-stress conditions.

The observed failure patterns indicate that the proposed CFRP anchoring system enhances the interfacial bond between the CFRP sheets and the concrete substrate, beyond the effect of external CFRP wrapping alone. This system contributes to stress redistribution under high loading conditions and alleviates stress concentrations at the specimen corners. Based on the failure modes of specimens S1, S2, and S3, it was found that when the number of anchors was limited (S1 and S2), the CFRP sheets exhibited significant tearing in the mid-height region, accompanied by partial anchor pullout. This indicates that the anchors were insufficient to prevent debonding of the CFRP, and that localized concrete damage further reduced the effectiveness of the confinement system. Following the rupture of the CFRP sheet, the confinement effect on the concrete core rapidly deteriorated, resulting in increased internal stress concentration, crack propagation, spalling of the concrete cover, and damage to the core. Mild buckling of the longitudinal reinforcement eventually led to structural instability. In contrast, specimen S3 demonstrated improved confinement performance throughout the loading process. No anchor pullout was observed, and cracks initiated at the anchor locations and extended toward the corners, suggesting that the anchoring system significantly enhanced the bond strength and promoted a more uniform stress distribution. Nevertheless, under extreme loading conditions, localized stress concentrations still led to interfacial failures around the anchors. For

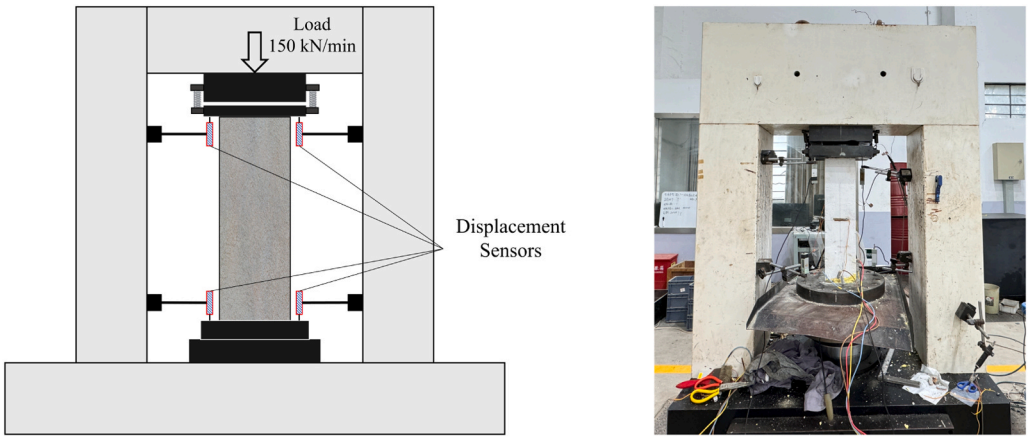

Fig. 5. Experimental loading setup.

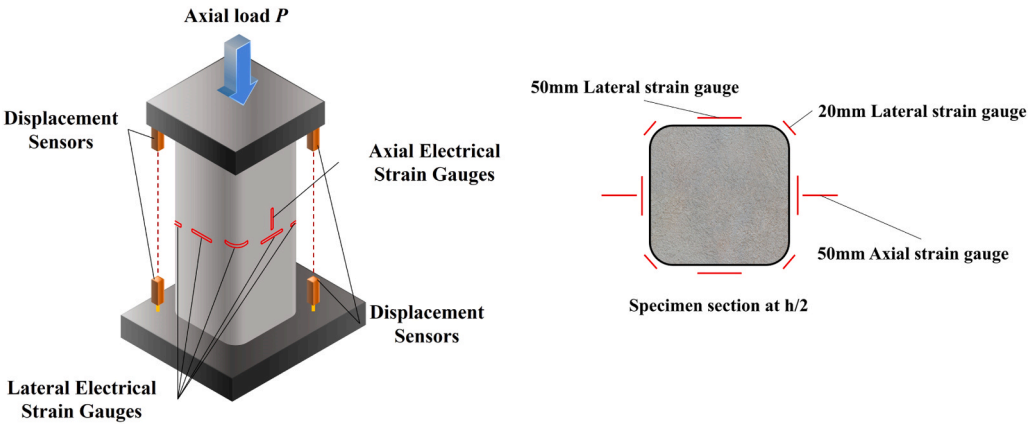

Fig. 6. The detailed layout of the displacement transducers and strain gauges.

specimen S4, with a further increase in the number of anchors, more pronounced local stress concentrations were observed near the anchors. The drilling required for anchor installation resulted in the formation of vertical penetrating cracks between adjacent anchors, which subsequently extended toward the corners. This indicates that excessive anchoring introduced stress-release paths that exacerbated CFRP sheet damage and reduced specimen integrity. As a result, the overall structural performance declined.

3.2. Load–displacement response

Fig. 8 presents the load–displacement responses of specimens strengthened with varying numbers of CFRP anchors under uniaxial compression. The control specimen UU, which was unconfined, exhibited the lowest peak load capacity (879.9 kN) and the smallest ultimate displacement. Its response curve demonstrated a typical brittle failure pattern, with a sharp decline in load immediately after reaching the peak. Specimen S0, confined only by externally wrapped CFRP sheets without anchors, showed a significantly higher peak load than UU, indicating that CFRP wrapping alone can effectively enhance the load-bearing capacity. However, due to the lack of anchorage, the post-peak drop remained steep, and the improvement in ductility was limited. As the number of CFRP anchors increased from S1 to S3, the load–displacement curves exhibited a clear enhancement trend. Both the peak load and ultimate displacement increased, with specimen S3 achieving the highest peak load in the test series (1333.2 kN) and exhibiting an extended plateau stage, reflecting the most favorable combination of strength and ductility. These results suggest that an appropriate number of CFRP anchors can significantly improve the bond between the CFRP and the concrete substrate, effectively delaying early debonding failures. Consistent with the observed failure modes, specimen S3 primarily experienced localized tearing of the CFRP and crack propagation near the anchors, while the concrete core remained largely intact. This indicates that the anchoring system facilitated more effective CFRP confinement and contributed to the development of a stronger compression–bending interaction and enhanced energy dissipation capacity through hysteretic behavior.

It is noteworthy that when the number of CFRP anchors was further increased to four (specimen S4), a degradation in performance was observed. The peak load slightly decreased to 1234.4 kN compared to S3, and the displacement capacity was also reduced. This decline is likely attributed to the excessive number of anchors compromising the integrity of the concrete, introducing numerous local stress concentration zones that triggered premature microcracking or localized failure. Additionally, overly dense anchor placement may result in non-uniform stress distribution within the CFRP sheets, adversely affecting the global force transfer and coordination. During the installation process, densely arranged anchors may also lead to localized debonding or stress interference, thereby reducing the confinement efficiency of the anchorage system. Therefore, based on the overall trend of the load–displacement curves, a moderate number of anchors (e.g., three) appears to offer an optimal balance—enhancing interfacial bond strength while preserving the structural integrity. This facilitates an effective synergy between load-bearing capacity and ductility, highlighting both the importance of optimized anchor layout and the nonlinear nature of strengthening effectiveness in CFRP anchoring systems.

3.3. Ductility analysis

Ductility refers to the deformation capacity of a structure after entering the inelastic stage, during which the load-bearing capacity does not significantly decrease prior to reaching the ultimate limit state. A higher ductility coefficient indicates superior deformability and energy absorption capacity, enabling the structure to undergo substantial plastic deformation before failure. In this study, the ductility coefficient is defined as the ratio of the peak displacement (Δ_u) to the yield displacement (Δ_y), as expressed in Eq. (1). Given that the yield point of CFRP-confined reinforced concrete short columns is not clearly distinguishable on the load–displacement curves, the "closest-to-line" method—currently considered a practical and reasonable approach—is employed to determine the yield point [39]. This method objectively identifies the yield without reliance on arbitrary offset parameters.

$$DI = \Delta_u / \Delta_y \tag{1}$$

Table 3 presents the variation in ductility coefficients for specimens with different strengthening configurations. It can be observed that specimens S0 and S1 exhibited higher yield and ultimate load capacities compared to the unconfined specimen UU; however, their ductility coefficients were lower. This indicates that while the use of externally bonded CFRP sheets or the addition of a single anchor can enhance load-bearing capacity, such configurations do not effectively improve, and may even slightly reduce, overall ductility. This reduction is primarily attributed to insufficient anchorage, which leads to interfacial debonding of the CFRP sheets during compressive deformation. As a result, the wrapping layer is unable to fully engage in energy dissipation during the post-yield stage, thereby limiting the development of ductility. Moreover, premature local failures induced by stress concentrations from partial debonding or slippage can further compromise the deformation capacity of the specimen. With the increase in the number of anchors, the ductility coefficients of specimens S2 and S3 were significantly improved, exhibiting a strong positive correlation between the anchorage quantity and ductility performance. In particular, specimen S3, characterized by a more uniform distribution of anchorage forces, demonstrated superior enhancement. This improvement indicates that,

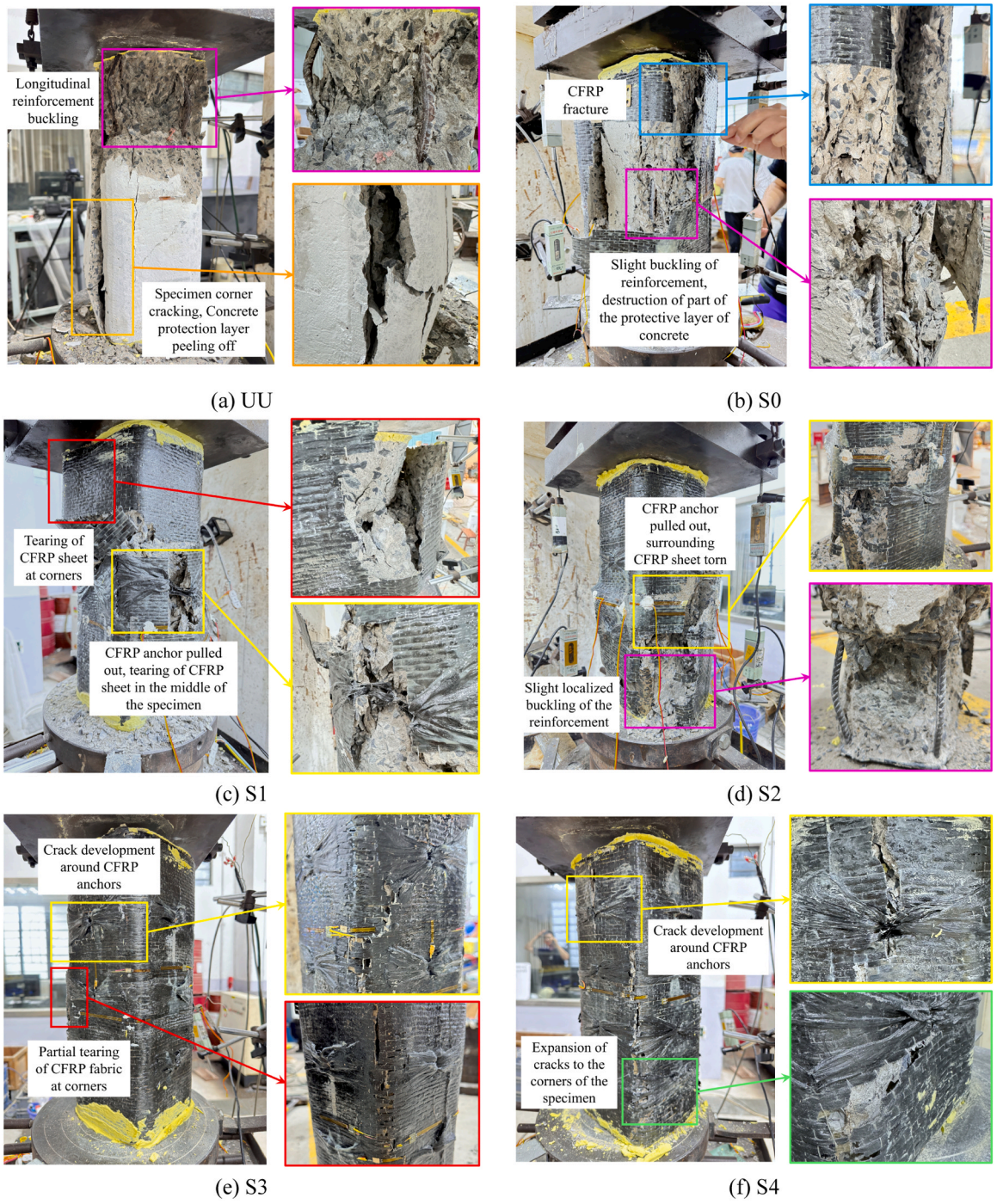

Fig. 7. Failure modes of specimens strengthened with different numbers of CFRP anchors.

once the number of anchors surpasses a critical threshold, a more robust and continuous bond interface between the CFRP sheets and the concrete is established, thereby strengthening the synergistic effect of the confinement mechanism.

When the number of anchors was further increased to four (specimen S4), the ductility coefficient declined, exhibiting a degradation trend similar to that observed in specimens S0 and S1. This suggests the existence of a "threshold" beyond which excessive anchor installation becomes detrimental. The primary cause lies in the disruption of structural integrity due to overly dense anchor placement, which can induce microcracks or localized stress concentrations in the core compression zone, leading to premature deterioration. Additionally, the anchor installation process reduces the effective cross-sectional area of the concrete through multiple drilled holes, thereby impairing its inherent plastic deformation capacity. Although S4 maintained a relatively high peak load, its ductility performance declined due to the unfavorable configuration. In summary, analysis of both load-bearing capacity and ductility coefficients indicates that the number and layout of CFRP anchors must strike a balance between enhancing interfacial bonding and preserving structural integrity. Only through this balance can simultaneous optimization of ductility and strength in the CFRP-strengthening system be achieved.

3.4. Constraint effect analysis

The load–displacement response data provide a basis for evaluating

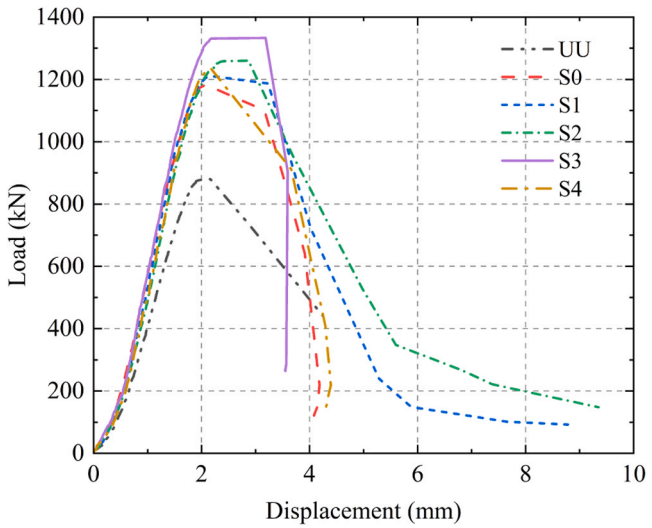

Fig. 8. Load–displacement curves of specimens strengthened with different numbers of CFRP anchors.

Table 3
Calculation results of ductility coefficients.

Columns	Yield load (kN)	Ultimate load (kN)	Ductility index	
			DI	DI_{Nor}[a]
UU	875.1	879.9	1.124314	1
S0	1182.9	1182.9	1	0.889431
S1	1211	1211	1	0.889431
S2	1258.2	1260	1.202684	1.069705
S3	1330.9	1333.2	1.461104	1.299551
S4	1234.4	1234.4	1	0.889431

[a] Normalized in relation to the column UU.

the confinement effectiveness of the CFRP anchoring system. Fig. 8 illustrates the variation curves of the strength improvement factor (SI) and the concrete strength enhancement coefficient (CSI) for different specimens. The strength improvement factor SI is defined as the ratio of the ultimate load to the nominal failure load, as expressed in Eqs. (2)-(4). The nominal failure load, calculated using Eq. (3), represents the combined contribution of the concrete and reinforcement under unconfined conditions. The SI thus reflects the synergistic interaction between steel reinforcement and concrete in enhancing the ultimate load-carrying capacity. In contrast, the concrete strength enhancement coefficient CSI is calculated to isolate the contribution of the concrete core by eliminating the influence of reinforcement. This parameter more accurately characterizes the enhancement in load resistance attributable solely to the confined concrete. The calculation method for CSI is also provided in the corresponding equations.

$$SI = N_u / N_0 \tag{2}$$

$$N_0 = f_y A_s + f_c' A_c \tag{3}$$

$$CSI = \frac{N_u - f_y A_s}{f_c' A_c} \tag{4}$$

Where A_s represents the cross-sectional area of the reinforcement (mm^2), A_c denotes the cross-sectional area of the concrete (mm^2), f_y is the tensile strength of the reinforcement (MPa), and f_c' is the axial compressive strength of cylindrical concrete specimens (MPa). The value of f_c' is calculated based on the empirical relationship $f_c' = 0.79 f_{cu,k}$ is the characteristic cube compressive strength of concrete.

Fig. 9 shows the variation of SI and CSI with the number of CFRP anchors. As shown in the figure, both SI and CSI exhibit a general trend

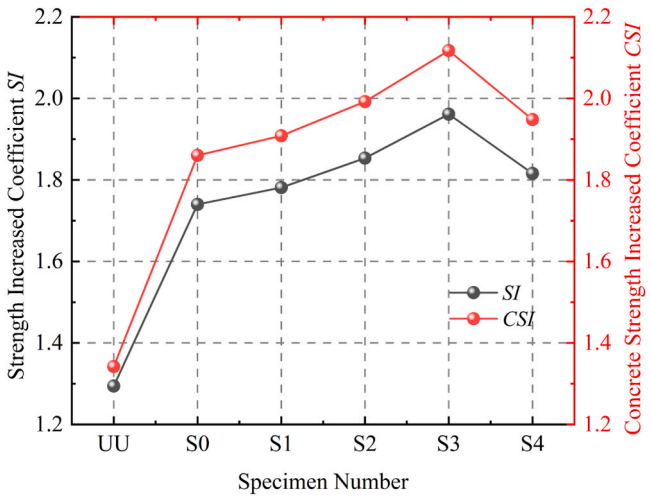

Fig. 9. Variation of SI and CSI with the number of CFRP anchors.

of increasing and then decreasing with the number of CFRP anchors, following a consistent pattern. This indicates that the anchors not only enhanced the confinement effectiveness of the external CFRP wrapping but also significantly improved the internal stress state of the concrete core, thereby contributing to both global and localized strength enhancement. A substantial increase in both SI and CSI was observed when transitioning from the unconfined specimen (UU) to the specimen wrapped with CFRP only (S0), suggesting that even in the absence of anchors, CFRP wrapping alone provides considerable lateral confinement, particularly in inducing a favorable triaxial compressive state within the concrete core. However, due to limitations in interfacial bond strength, the confinement effect remains somewhat constrained. As the number of anchors increased from 1 to 3, both SI and CSI continued to rise, reaching their peak values in specimen S3. This indicates that the synergistic action of the CFRP sheets and multiple anchors enables more effective stress transfer into the concrete core, transforming the internal stress state from biaxial to triaxial compression, and thereby significantly enhancing core concrete strength. Moreover, multiple anchorage points suppressed crack propagation and mitigated debonding, contributing to improved structural integrity and stability, and fully leveraging the advantages of the composite strengthening system. When the number of anchors was further increased to four, both SI and CSI showed a noticeable decline. This degradation trend is consistent with the previously observed reductions in ductility coefficient and changes in the load–displacement response. Excessive anchorage can compromise the structural integrity of the concrete, complicate the stress distribution within the CFRP sheets, and introduce local stress concentrations, warping, or stress interference, which may hinder further enhancement of concrete strength.

3.5. Stress–strain response

Fig. 10 illustrates the axial stress–strain curves of reinforced concrete columns strengthened with different numbers of CFRP anchors. The curves exhibit a typical nonlinear ascending trend. UU showed the lowest ultimate strength and the poorest plastic deformation capacity. With the introduction of CFRP wrapping and anchor reinforcement from specimens S0 to S3, the curves progressively shifted upward. Notably, specimen S3 demonstrated superior performance, with an ultimate stress exceeding 60 MPa and a steep yet extended stress–strain response, indicating both high strength and enhanced deformability. This suggests that the anchoring system effectively established a triaxial confinement state in the concrete core, enabling the specimen to rapidly carry axial loads while maintaining favorable strain adaptability throughout loading. Furthermore, the presence of anchors prevented premature

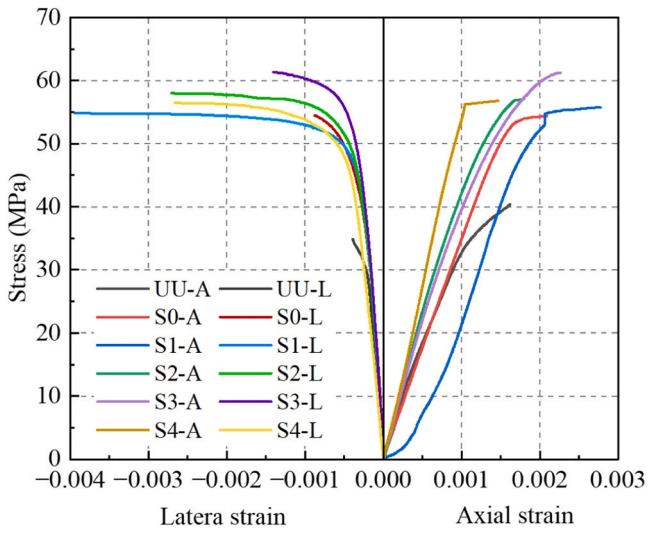

Fig. 10. Stress–strain curves of specimens strengthened with different numbers of CFRP anchors.

debonding of the CFRP sheets and alleviated local stress concentrations, allowing the confinement layer to fully participate in axial load resistance.

The hoop stress–strain curves directly reflect the development of lateral confinement within the specimens. For specimens UU and S0, insufficient restraint of lateral concrete expansion led to rapid stress release in the core region, resulting in relatively low hoop stresses. As the number of CFRP anchors increased from S1 to S3, the hoop stress was continuously enhanced. In particular, specimens S2 and S3 exhibited significant increases in hoop stress, with steeper curve profiles, indicating that higher lateral confinement was generated within the core. This effectively suppressed lateral dilation of the concrete and contributed to improved compressive strength of the overall structure. However, in comparison, although specimen S4 still maintained relatively high axial and hoop stresses, both values decreased slightly relative to S3. This suggests that the additional anchors did not continue to improve performance. Instead, the excessive anchor density may have induced local cracking or stress overlap within the concrete, limiting the effectiveness of the CFRP confinement. At the same time, the measured maximum circumferential strain of the S1-S4 group CFRP sheath is lower than the manufacturer's provided ultimate tensile strain (0.001), which is 29.07 %, 36.90 %, 71.43 %, and 37.45 %, respectively. This indicates that the introduction of CFRP anchor rods effectively prevents CFRP from reaching its fracture strain, thereby improving the constraint efficiency. Notably, the hoop stress in S4 did not surpass that of S3 and even exhibited a plateauing trend. This indicates the onset of interfacial debonding and localized damage, which ultimately weakened the effectiveness of the strengthening system.

To evaluate the effectiveness of the CFRP anchoring system in providing lateral confinement, multiple strain gauges were installed at the mid-height section of each specimen. Fig. 11 presents the hoop strain distribution for specimens strengthened with varying numbers of anchors. Overall, the control specimen (UU) and the specimen strengthened without anchors (S0) exhibited strain fluctuations as early as 60 % P_{max} and 70 % P_{max}, respectively. In contrast, specimens with anchorage reinforcement maintained relatively stable hoop strain distributions up to 90 % P_{max} and 100 % P_{max}, with strain values increasing uniformly across the section. This indicates that the anchoring system enables greater development of lateral strain, improved deformation compatibility, and enhanced confinement stability—factors that are critical to improving structural ductility and delaying failure onset. At 100 % P_{max}, the strain distribution in specimen S1 appeared smoother compared to UU and S0, with peak strain values symmetrically located across the section. Although a single anchor was insufficient to establish a fully integrated confinement network, it contributed to improved bonding of the CFRP sheets and mitigated early debonding. However, the axial stress-strain curve of the S1 specimen exhibits different initial stiffness, mainly due to the limited constraint provided by a single anchor point, resulting in uneven stress transfer during the early loading stage. Specimens S2 and S3 exhibited more uniform and regular strain distributions, especially S3, where most measurement points maintained high and relatively even strain levels under peak load. The maximum strain was observed at the mid-section rather than at the corners, indicating that the anchoring system effectively alleviated the common issue of stress concentration at corners in CFRP-strengthened rectangular columns. This demonstrates the system's superior deformation compatibility and its ability to promote efficient composite action between CFRP and concrete.

Fig. 12 compares the hoop strain distributions of specimens strengthened with different numbers of CFRP anchors under 100 % P_{max} loading. For specimen S0, which was confined using CFRP sheets without anchors, the measured strain values remained relatively low and evenly distributed, with no significant fluctuations. This indicates that, under high loading conditions, the confinement effect of the CFRP layer was not effectively mobilized due to insufficient interfacial bonding. In conjunction with the load–displacement data, this uniform but low-level response does not signify efficient structural behavior, but rather reflects the underperformance of the confinement system and the limited contribution of CFRP to load resistance. In contrast, specimens S1 through S4, all equipped with CFRP anchors, showed a marked increase in hoop strain levels with increasing anchor quantity. This demonstrates that the anchors significantly enhanced the interfacial bond between the CFRP and the concrete substrate, enabling the wrapping layer to more fully engage in lateral confinement under high axial loads. Among all strengthened specimens, S3 exhibited the most favorable strain distribution. The strain curve showed minimal fluctuation, consistently high values, and small differences among measurement points, indicating that a stable and continuous lateral confinement mechanism was established under peak loading. Although specimen S4 had a higher number of anchors, its strain distribution curve exhibited pronounced peaks and troughs. While no severe stress concentration occurred at the corners, a sudden stress drop was observed at the mid-section anchor location (X5), suggesting that excessive anchor density introduced stress interference and local instability between anchor points. This further confirms the presence of an "optimal anchor configuration" threshold within the CFRP confinement system.

In conclusion, the experimental data clearly reveal the deformation control capacity and confinement synergy offered by the CFRP anchoring system. Compared with traditional FRP wrapping methods, the CFRP anchoring system demonstrates superior confinement coordination and structural adaptability. An appropriate number of anchors—such as in specimen S3—strikes a balance between enhancing confinement stress, improving core concrete strength, and achieving coordinated stress transfer. This enables the member to develop high strength while maintaining favorable ductility and toughness, thereby establishing a desirable structural response characterized by strong confinement, high load-bearing capacity, and gradual failure progression. In contrast, insufficient or excessive anchorage may lead to unbalanced interfacial bonding or localized stress concentrations, which weaken the effectiveness of the confinement. This results in uneven hoop deformation and degradation of the overall mechanical performance of the structure.

4. Stress-strain model

4.1. Existing model

At present, numerous stress–strain models have been proposed for FRP-confined reinforced concrete columns subjected to axial loading.

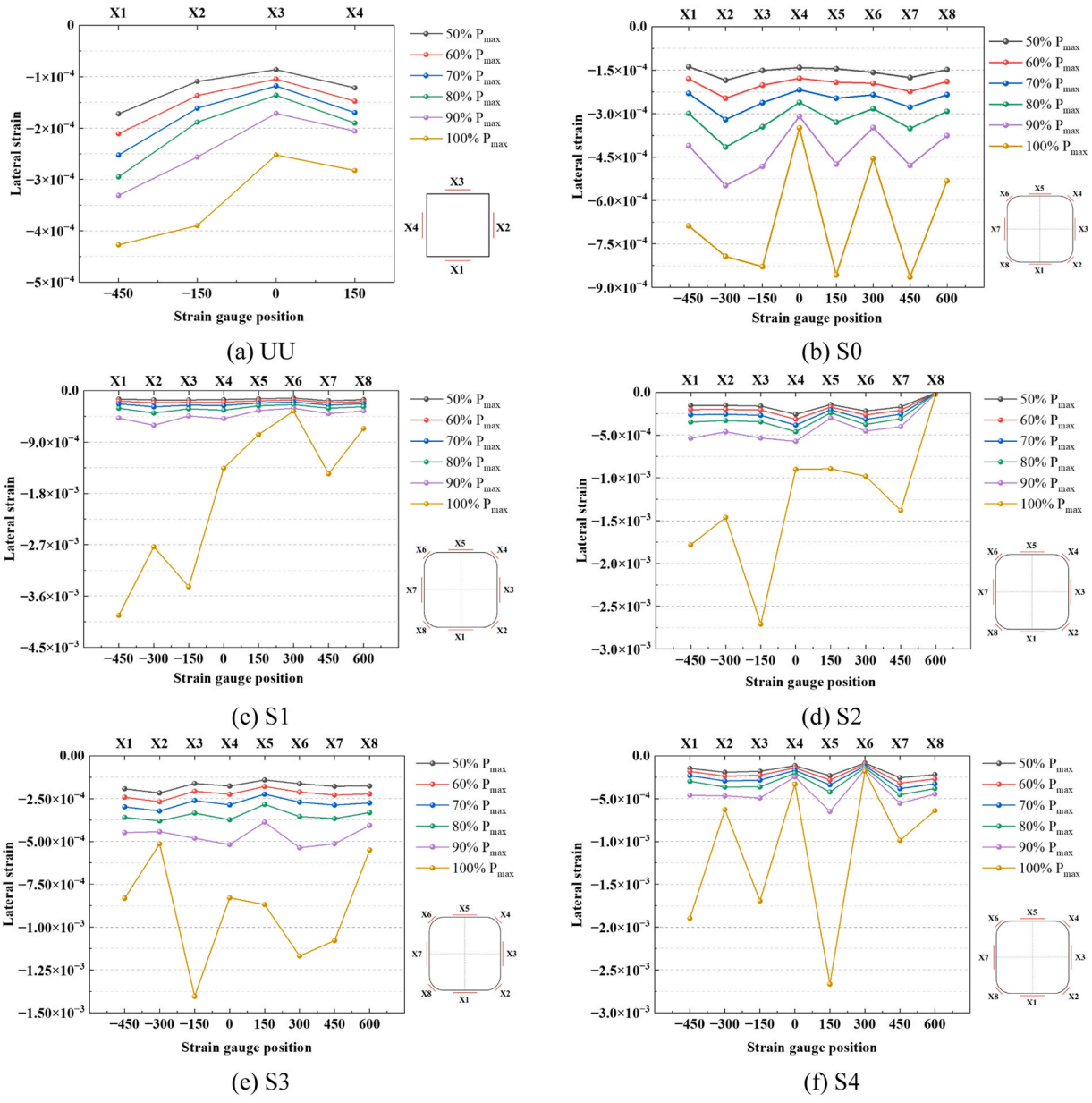

Fig. 11. Distribution of hoop strain in specimens strengthened with different numbers of CFRP anchors.

Youssef et al. developed a two-stage stress–strain model to predict the behavior of FRP-confined columns with circular and rectangular cross-sections [40]. Teng' group subsequently proposed models for the ultimate stress and strain of columns with different cross-sectional shapes [41,42]. Fig. 13 illustrates typical bilinear and post-peak softening stress–strain response models commonly used in the literature. For structures under strong confinement provided by CFRP anchoring systems, the bilinear model is frequently adopted. This model is divided into two segments at the transition point (ε_{cc}', f_{cc}'): the first segment represents a parabolic curve prior to the transition point, and the second segment is a linear curve extending beyond the transition point. In this study, the monotonic stress–strain model proposed by Zhou and Wu [31], which incorporates four fitting parameters, was adopted to simulate the axial stress–strain behavior of CFRP-anchor-confined reinforced concrete square columns.

$$f_c = \left[(E_1\varepsilon_n - f_o)e^{-\frac{\varepsilon_c}{\varepsilon_n}} + f_o + E_2\varepsilon_c\right]\left(1 - e^{-\frac{\varepsilon_c}{\varepsilon_n}}\right) \tag{5}$$

Where f_o denotes the stress limit in the elastic stage of the stress–strain relationship. For the highly confined concrete specimens discussed in this study, f_o is taken as f_{co}, i.e., f_o=f_{co}. E_1 represents the initial stiffness of the stress–strain curve, and based on regression results from relevant literature, it can be expressed as $E_1 = 5573 f_{co}^{0.5}$. The parameter n primarily controls the curvature of the transition zone and ranges between 0 and 1. The confinement ratio has an insignificant effect on n, and a value of $n = 0.76$ is adopted based on regression analysis. The corresponding strain ε_n is calculated as ε_n=$n \times \varepsilon_0$, where ε_0=f_o/E_1. E_2 denotes the slope of the asymptotic hardening branch for the stress–strain relationship of highly confined concrete. According to the findings of this study, E_2 is computed using the following equation:

$$E_2 = \frac{f_{cc} - f_o}{\varepsilon_{cc}} = \frac{f_{cc} - f_{co}}{\varepsilon_{cc}} \tag{6}$$

Where f_{cc} represents the peak stress, and ε_{cc} denotes the peak strain. The specific values of these parameters are determined based on the findings presented in Section 4.2 of this study.

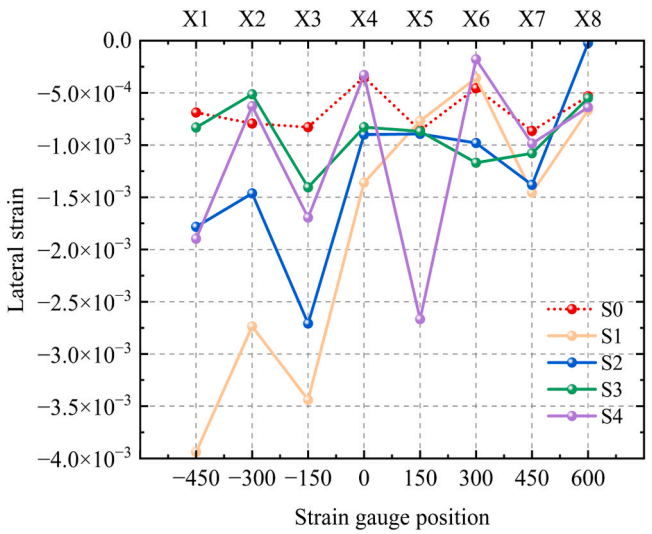

Fig. 12. Comparison of hoop strain distribution in specimens under 100 % Pmax loading level.

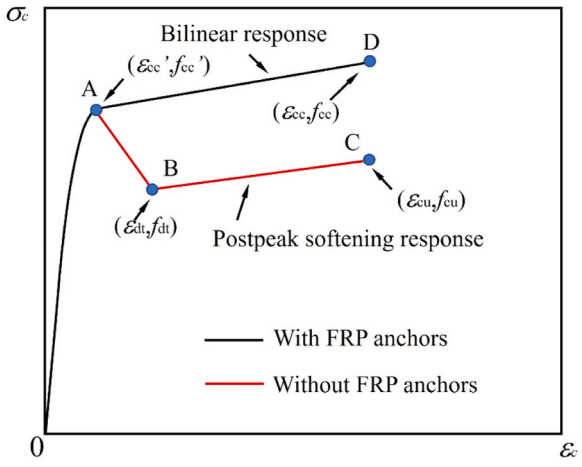

Fig. 13. Typical stress–strain models of FRP-confined concrete with strain hardening behavior.

4.2. Lateral confining stresses

For reinforced concrete square columns strengthened with CFRP anchoring systems, the lateral confinement under uniaxial compression is primarily provided by three sources: external CFRP wrapping (f_{lfe}), CFRP anchors (f_{la}), and transverse steel reinforcement (f_{ls}). In this study, the theoretical model proposed by Isleem et al. [37] is adopted to calculate and incorporate the effects of these three confinement components. The following sections provide a detailed discussion of each parameter.

(1) Confining pressure by external CFRP wraps

The effective confinement provided by the external CFRP wrapping is calculated using the following equation:

$$f_{lfe} = k_{ef}\rho_{fw}f_f \tag{7}$$

Where f_f is the ultimate tensile strength of the unidirectional CFRP sheet, and ρ_{fw} is the volumetric ratio of the CFRP wrapping, calculated as $\rho_{fw}= 4n_f t_f/D$, where $D= 2bh/b+h$ (mm) is the equivalent diameter of a rectangular cross-section, n_f is the number of CFRP layers, and t_f is the thickness of a single CFRP layer. The shape factor k_{ef} for a rectangular section is calculated using the following expression. In this context, A_{cf} and A_g (mm^2) denote the effectively confined concrete area and the gross cross-sectional area of the chamfered rectangular column, respectively:

$$k_{ef} = \frac{A_{cf}}{A_g} \tag{8}$$

$$A_{cf} = \begin{cases} A_g - \dfrac{(b-2r_c)^2+(h-2r_c)^2}{3}; \dfrac{(h-2r_c)}{4} \le \dfrac{b}{2} \\ A_g - \dfrac{(b-2r_c)^2+(h-2r_c)^2}{3} + \dfrac{4}{3}h_0\sqrt{\dfrac{(h-2r_c)h_0}{2}}; \dfrac{(h-2r_c)}{4} \ge \dfrac{b}{2} \end{cases} \tag{9}$$

$$A_g = bh - (4-\pi)r_c^2 \tag{10}$$

(2) Confinement pressure by FRP anchors

The lateral confinement stress provided by CFRP anchors is calculated using a recently proposed model by Isleem et al.:

$$f_{la} = k_{ea}\rho_{fa}f_f \tag{11}$$

$$\rho_{fa} = \left(\frac{A_{a,y}}{hH'} + \frac{A_{a,x}}{bH'}\right) \times \left(\frac{D^*}{D}\right) \tag{12}$$

$$H' = (r_a - 1) \times s_a \tag{13}$$

$$\begin{cases} A_{a,x} = (c \times r \times a)_x \\ A_{a,y} = (c \times r \times a)_y \end{cases} \tag{14}$$

$$\begin{cases} a_x = w_{a,x} \times t_{a,x} \\ a_y = w_{a,y} \times t_{a,y} \end{cases} \tag{15}$$

Where ρ_{fa} represents the equivalent ratio of CFRP anchors, which accounts for the confinement effects along both the longer and shorter sides of the cross-section. In this study, square-section columns are considered, where b=h, and the equivalent diameter is given as $D^*= (b+h)^{1/2}$. $A_{a,y}$ and $A_{a,y}$ (mm^2) refer to the cross-sectional areas of anchors oriented perpendicular to the long and short sides of the section, respectively. c and r denote the number of anchors placed perpendicular and parallel to the section sides. w and t are the width and thickness of a single folded CFRP anchor, respectively. Given that the anchors in this study are symmetrically and uniformly distributed, it is assumed that $A_{a,y}$=$A_{a,y}$. The confinement efficiency of the CFRP anchors, k_{ea}, is calculated using the following equation:

$$k_{ea} = \frac{A_{ca}}{A_g} = \frac{A_{c.f.a} - A_{cf}}{A_g} \tag{16}$$

$$A_{c.f.a} = A_g - \frac{(h-2r_c)(h-2r_c+1.5c_{a,y}s_a) + (c_{a,y}+1)(b-2r_c)^2}{3(c_{a,y}+1)} \tag{17}$$

Where $A_{c.f.a}$ denotes the total cross-sectional area effectively confined by the CFRP anchoring system. The parameters A_{cf} and A_g are calculated using the corresponding expressions provided earlier. In this model, the fan-shaped portion of the CFRP anchors is assumed to extend the effective confinement region around the anchor location, thereby enhancing the stiffness of the CFRP wrapping layer. Accordingly, the vertical spacing between anchors is assumed to be s_a= 0.

(3) Confinement pressure by steel hoops

The lateral confinement pressure provided by transverse stirrups is calculated using the following equation:

$$f_{ls} = \rho_{sv}f_{yv} \tag{18}$$

$$\rho_{sv} = \frac{A_{shx} + A_{shy}}{s'(b+h)} \tag{19}$$

Where ρ_{sv} denotes the equivalent volumetric ratio of the transverse stirrups, and f_{yv} is the yield strength of the stirrup steel. A_{shx} and A_{shy} (mm^2) represent the cross-sectional areas of stirrups along the longer and shorter sides of the section, respectively. In this study, A_{shx}=A_{shy}= 8 mm^2.

(4) Combined confinement from FRP wraps and anchors and the steel hoops

Building upon the confinement model developed by Isleem et al. for predicting the ultimate strength of FRP-anchor-confined rectangular RC columns, this study introduces a modification based on experimental observations. Specifically, a reduction function η(n), dependent on the number of anchors n on a single side, is incorporated to account for the potential weakening of confinement effectiveness caused by the drilling process during CFRP anchor installation. This adjustment enhances the predictive accuracy of the model for specimens strengthened with CFRP anchoring systems. The modified confinement model is expressed as follows:

$$\frac{f_{cc}}{f_c'} = \eta(n)(0.730 + 2.773\mathrm{MC_R}) \tag{20}$$

$$\mathrm{MC_R} = \left[\frac{3.109(f_{ls})^{1.671} + 0.039\left(f_{la}+f_{lfe}\right)^{2.852}}{f_c'}\right]^{1.187} \tag{21}$$

$$\eta(n) = -9.417\left(1 - \frac{4A_H}{A_C}\right)^{n} - 0.599n + 10.35 \tag{22}$$

Where $\mathrm{MC_R}$ is a dimensionless parameter introduced to account for the combined contribution of internal transverse reinforcement and the FRP anchoring system to the peak strength. n denotes the number of anchors on one side of the column. A_H is the cross-sectional area of the drilled anchor holes, calculated as A_H=r_H×d_H, where r_H is the hole diameter and d_H is the hole depth. A_C represents the effective cross-sectional area of the concrete. The peak strength of the specimen is calculated based on the theoretical model proposed by Li et al., with parameters α_1 and α_2 modified in this study to improve accuracy.

$$\frac{f_{cc}'}{f_{cc}} = \alpha_1\alpha_2\exp\left[-0.144\left(\frac{f_{ls}+f_{la}+f_{lfe}}{f'_c}\right)^{-0.503}\right] \tag{23}$$

$$\alpha_1 = \left(0.8 + 0.2\frac{25}{f_c'}\right)^{0.041} \tag{24}$$

$$\alpha_2 = \exp\left[0.426\left(\frac{f_c'}{f_{cc}}\right)^{1.812}\right] \tag{25}$$

Where f_c' denotes the unconfined concrete compressive strength, which is estimated using the empirical relation f_c'= 0.79 f_c.

4.3. Calculation results of the modified model

Table 4 presents the predicted ultimate stresses calculated using the modified Isleem model. It can be observed that the discrepancies between the theoretical and experimental results are relatively small. The coefficients of determination (R^2) for both the transition peak stress (f_{cc}') and the peak stress (f_{cc}) exceed 87 %, indicating a high level of predictive accuracy. Moreover, the reduction function proposed in this study effectively captures the decline in ultimate stress associated with excessive anchor quantity.

Based on the calculated peak stress and corresponding strain, the theoretical stress–strain curves were generated using the model proposed by Zhou and Wu, as shown in Fig. 14. A comparison between the experimental and theoretical stress–strain responses of the four specimens strengthened with CFRP anchoring systems reveals that the model effectively captures the overall development trend of the confined concrete behavior. In particular, good linear consistency is observed in the parabolic segment prior to the transition point, especially as the number of anchors increases. The decreasing deviation between theoretical and experimental curves in this region indicates that the model can reasonably simulate the bond–slip behavior and anchorage force transfer at the FRP–concrete interface, with high accuracy in predicting the stiffness during the elastic stage. In all specimens (S1–S4), the theoretical stress–strain curves consistently fall slightly below the experimental data within the linear stage, indicating that the analytical model underestimates the strengthening effect of the CFRP anchorage system. This situation suggests that the CFRP-anchored reinforced concrete columns sustain higher stress while maintaining progressive strain development, highlighting their superior ductility in the mid-to-late loading stages. Such behavior can be attributed to the synergistic action of the CFRP confinement and anchorage, which delays stiffness degradation, redistributes localized stresses, and mitigates premature failure. Consequently, the anchorage system exhibits a more pronounced contribution to energy dissipation and post-yield deformability than predicted by the theoretical formulation, underscoring its structural efficiency in improving both strength and ductility performance.

5. Conclusions

This study systematically investigated the mechanical performance of reinforced concrete (RC) square columns strengthened with CFRP anchoring systems and developed a stress–strain prediction model that accounts for the influence of anchor quantity. Both experimental results and theoretical analyses highlight the critical role of the anchoring system in enhancing confinement efficiency, improving interfacial bonding, and upgrading structural performance. The main conclusions are as follows:

(1) The CFRP anchoring system significantly modified the failure mechanisms of RC square columns. As the number of anchors increased, failure modes transitioned from brittle global instability to localized ductile damage. Specimen S3 (three anchors) exhibited restrained concrete spalling, reduced longitudinal bar buckling, and more distributed crack patterns, indicating enhanced structural integrity.

(2) Both load–displacement and stress–strain responses demonstrated that a moderate number of anchors markedly improved strength and ductility. Specimen S3 showed the highest peak load (1333.2 kN) and ductility index (1.46), with hoop strain distribution becoming more uniform and symmetric, reflecting effective triaxial confinement and energy dissipation capacity.

(3) A modified stress–strain model was developed, incorporating a

Table 4
Theoretical calculation results of peak stress and ultimate stress.

Specimen	f_{cc}'^{e}	f_{cc}'^{r}	R^2	f_{cc}^{e}	f_{cc}^{r}	R^2
S1	53.09417	52.30070	87.30 %	55.73599	56.05963	90.87 %
S2	53.51943	53.70573		57.13054	57.22560	
S3	57.22719	56.09928		61.25436	61.99851	
S4	51.10003	50.31753		56.81297	57.78188	

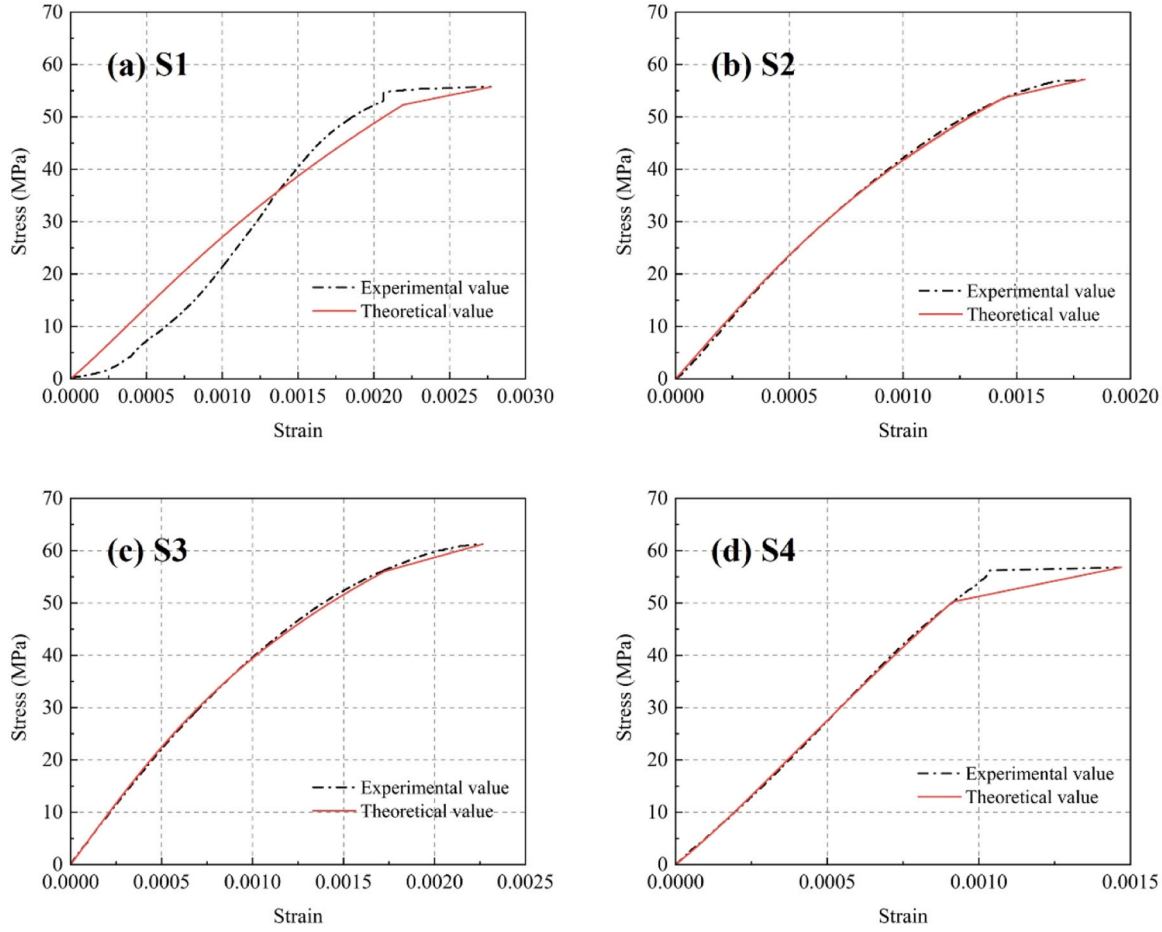

Fig. 14. Comparison between theoretical and experimental stress–strain curves.

reduction function that accounts for confinement loss due to anchor installation. The model accurately predicted the mechanical response, with R^2 values exceeding 87 % for both peak and ultimate stresses. It effectively captures the nonlinear strengthening behavior before and during loading and provides a reliable design tool for CFRP-confined RC columns with anchors.

CRediT authorship contribution statement

Xubing Xu: Methodology, Investigation. **Xin Lan:** Methodology, Investigation. **Chao Yang:** Validation, Investigation. **Liangqin Wu:** Validation, Methodology. **Yubao Zhou:** Validation, Investigation. **Zhengxie Zhang:** Writing – original draft, Methodology, Investigation, Conceptualization. **Tanbo Pan:** Writing – review & editing, Methodology, Investigation. **Yonglai Zheng:** Supervision, Funding acquisition. **Chenyu Hou:** Software, Investigation.

Declaration of Competing Interest

The authors declare that they have no known competing financial interests or personal relationships that could have appeared to influence the work reported in this paper.

Acknowledgments

The authors acknowledge financial support from the National Natural Science Foundation of China (No. 52468023) , the Early Career Youth Science and Technology Talent Training Program of Jiangxi Province (No. 20244BCE52161), and the Natural Science Foundation of Jiangxi Province, Youth Program (No. 20252BAC200092).

Data availability

Data will be made available on request.

References

[1] Koutas L, Triantafillou TC. Use of anchors in shear strengthening of reinforced concrete T-Beams with FRP. J Compos Constr 2013;17(1):101–7.
[2] Long NM, Phuong PV, Duong TT, Truong QPT, Pham TM, Cuong NH, Rovnák M. Flexural-strengthening efficiency of cfrp sheets for unbonded post-tensioned concrete T-beams. Eng Struct 2018;166:1–15.
[3] Kaeseberg S, Messerer D, Holschemacher K. Assessment of standards and codes dedicated to CFRP confinement of RC columns. Materials 2019;12(15).
[4] Erki MA. Fiber-Reinforced polymers for structural engineering in Canada. R Mil Coll Can Kingston Can 1999;9(4):278–81.
[5] Hollaway LC, Leeming MB. Strengthening of reinforced concrete structures using externally bondad FRP composites in structyral and civil engineering. Rev De Metal 2000;36(6).
[6] Taerwe LR, Matthys S. FRP for concrete construction: activities in Europe. Concr Int 1999;21(10):33–6.
[7] Zeng JJ, Liao JJ, Ye YY, Guo YC, Zheng Y, Tan LH. Behavior of FRP spiral strip-confined concrete under cyclic axial compression. Constr Build Mater 2021;295.
[8] Du YS, Zhang YT, Chen ZH, Yan JB, Zheng ZH. Axial compressive performance of CFRP confined rectangular CFST columns using high-strength materials with moderate slenderness. Constr Build Mater 2021;299.
[9] Bai YL, Dai JG, Teng JG. Buckling of steel reinforcing bars in FRP-confined RC columns: an experimental study. Constr Build Mater 2017;140:403–15.
[10] Al-Nimry H, Neqresh M. Confinement effects of unidirectional CFRP sheets on axial and bending capacities of square RC columns. Eng Struct 2019;196.
[11] Fan LL, Jin L, Zhao O, Liang J, Li P, Du XL. Plastic hinge behavior of rectangular CFRP-confined RC columns: Meso-scale modelling and formulation. Eng Struct 2024;307.

[12] Fan LL, Jin L, Du XL. Effects of structural size and corner radius on eccentric failure of rectangular CFRP-wrapped RC columns: Meso-scale modellings. Eng Struct 2023;283.
[13] Rehman AU, Siddiqi ZA, Yasin M, Aslam HMS, Noshin S, Aslam HMU. Experimental study on the behavior of damaged CFRP and steel rebars RC columns retrofitted with externally bonded composite material. Adv Compos Mater 2025;34(1):93–139.
[14] Castro VJ, León FJ, Martínez S, de Diego A, Echevarría L. Effectiveness of CFRP jackets in RC rectangular columns. Full-scale experimental study. Constr Build Mater 2024;416.
[15] Narule GN, Bambole AN. Axial behavior of CFRP wrapped RC columns of different shapes with constant slenderness ratio. Struct Eng Mech 2018;65(6):679–87.
[16] dos Santos LS, Damasceno IIR, Ribeiro LCN, de Oliveira DRC. Rounded corners columns strengthened with CFRP. Acta SciTechnol 2013;35(3):463–8.
[17] Vivekanandan R, Aarthi K. Behavior of hybrid FRP strengthened RC column under axial compression. IjstT Civ Eng 2023.
[18] Balla TMR, Prakash SS, Rajagopal A. Role of size on the compression behaviour of hybrid FRP strengthened square RC columns-Experimental and finite element studies. Compos Struct 2023;303.
[19] Saeed YM, Aules WA, Rad FN. Post-strengthening rapid repair of damaged RC columns using CFRP sheets for confinement and NSM-CFRP ropes for flexural strengthening. Structures 2022;43:1315–33.
[20] Saleem S, Shah OH, Jirawattanasomkul T, Zhang DW, Pimanmas A, Kunawisarut A, Srivaranun S. Evaluating natural and synthetic fibers in strengthening concrete column specimens with varying corner radii and aspect ratios. J Build Eng 2025;103.
[21] Kunawisarut A, Jongvivatsakul P, Jirawattanasomkul T, Likitlersuang S. Experimental study and modeling of unidirectional jute FRP for concrete confinement. Structures 2024;67.
[22] Zhong Y, Wang YL, Chen GP, Liu FG. Axial compressive performance and modeling of rectangular FRP-concrete-HSS hybrid multi-tube concrete columns. Structures 2025;73.
[23] Yardim Y, Yilmaz S, Corradi M, Thanoon WA. Strengthening of reinforced concrete Non-Circular columns with FRP. Materials 2023;16(21).
[24] Mercimek Ö, Ghoroubi R, Anil Ö, Çakmak C, Özdemir A, Kopraman Y. Strength, ductility, and energy dissipation capacity of RC column strengthened with CFRP strip under axial load. Mech Based Des Struc 2023;51(2):961–79.
[25] Aules W, Saeed YM, Rad FN. A novel anchorage system for strengthening slender RC columns with externally bonded CFRP composite sheets. Constr Build Mater 2020;245.
[26] Ghoroubi R, Mercimek Ö, Özdemir A, Anil Ö. Experimental investigation of damaged square short RC columns with low slenderness retrofitted by CFRP strips under axial load. Structures 2020;28:170–80.
[27] Zhang HW, Smith ST, Kim SJ. Optimisation of carbon and glass FRP anchor design. Constr Build Mater 2012;32:1–12.
[28] Triantafillou TC, Choutopoulou E, Fotaki E, Skorda M, Stathopoulou M, Karlos K. FRP confinement of wall-like reinforced concrete columns. Mater Struct 2016;49(1-2):651–64.
[29] Gao P, Yuan DM, Chen ZH, Mosallam AS, Tao C, Wang MQ. SEISMIC performance of RC square columns strengthened by bidirectional basalt-fiber-reinforced polymer (BFRP) composite laminates with fan-shaped anchors. Constr Build Mater 2023;406.
[30] Tasdemir E, Seracino R, Kowalsky MJ, Nau J. Behavior of large diameter carbon fiber anchors. Constr Build Mater 2023;394.
[31] Zhou YW, Wu YF. General model for constitutive relationships of concrete and its composite structures. Compos Struct 2012;94(2):580–92.
[32] Castillo ED, Griffith M, Ingham J. Seismic behavior of RC columns flexurally strengthened with FRP sheets and FRP anchors. Compos Struct 2018;203:382–95.
[33] Bournas DA, Pavese A, Tizani W. Tensile capacity of FRP anchors in connecting FRP and TRM sheets to concrete. Eng Struct 2015;82:72–81.
[34] Hany NF, Hantouche EG, Harajli MH. Generalized axial Stress-Strain response of rectangular columns confined using CFRP jackets and anchors. J Compos Constr 2017;21(1).
[35] Lin G, Teng JG. Advanced stress-strain model for FRP-confined concrete in square columns. Compos Part BEng 2020;197.
[36] Isleem HF, Tahir M, Wang ZY. Axial stress-strain model developed for rectangular RC columns confined with FRP wraps and anchors. Structures 2020;23:779–88.
[37] Isleem HF, Wang Z, Wang D. A new model for reinforced concrete columns strengthened with fibre-reinforced polymer, PhD candidate, key lab of structures dynamic behaviour and control of the ministry of education (Harbin Institute of Technology) professor. Key Lab Struct Dyn Behav Control Minist Educ (Harbin I 2020;173(8):602–22.
[38] Kim S, Smith S. Pullout strength models for FRP anchors in uncracked concrete. J Compos Constr 2010;14(4):406–14.
[39] Feng P, Cheng S, Bai Y, Ye L. Mechanical behavior of concrete-filled square steel tube with FRP-confined concrete core subjected to axial compression. Compos Struct 2015;123(0):312–24.
[40] Youssef MN, Feng MQ, Mosallam AS. Stress–strain model for concrete confined by FRP composites. CA 92697-2175, USA Dep Civ Environ Eng Univ Calif Irvine 2007;38(5-6):614–28.
[41] J. Teng, L. Lam, Compressive Behavior of Carbon Fiber Reinforced Polymer-Confined Concrete in Elliptical Columns, [1] Hong Kong Polytech Univ, Dept Civil & Struct Engn, Hong Kong, Hong Kong, Peoples R China Vol.128(No.12) (2002) 1535-1543.
[42] Lam L, Teng J. Strength models for Fiber-Reinforced Plastic-Confined concrete. J Struct Eng 2002;128(5):612–23.